

A modal approach for the efficient analysis of a bionic multi-layer sound absorption structure

Yonghua Wang^{*1}, Chengyu Xu¹, Yanling Wan¹,
Jing Li¹, Huadong Yu¹ and Luquan Ren²

¹ College of Mechanical and Electric Engineering,
Changchun University of Science and Technology, Changchun 130022, P.R. China
² Key Laboratory of Bionic Engineering (Ministry of Education),
Jilin University, Changchun 130022, P.R. China

(Received September 10, 2015, Revised March 14, 2016, Accepted March 18, 2016)

Abstract. The interest of this article lies in the proposition of using bionic method to develop a new sound absorber and analyze the efficient of this absorber in a ski cabin. Inspired by the coupling absorption structure of the skin and feather of a typical silent flying bird – owl, a bionic coupling multi-layer structure model is developed, which is composed of a micro-silt plate, porous fibrous material and a flexible micro-perforated membrane backed with airspace. The finite element simulation method with ACTRAN is applied to calculate the acoustic performance of the multi-layer absorber, the vibration modal of the ski cabin and the sound pressure level (SPL) near the skier's ears before and after pasting the absorber at the flour carpet and seats in the cabin. As expected, the SPL near the ears was significantly reduced after adding sound-absorbing material. Among them, the model 2 and model 5 showed the best sound absorption efficiency and the SPL almost reduced 5 dB. Moreover, it was most effective for the SPL reduction with full admittance configuration at both the carpet and the seats, and the carpet contribution seems to be predominant.

Keywords: biomimetic method; multi-layer absorber; modal analysis; sound pressure level; acoustic admittance

1. Introduction

In recent years, the need for increased audible comfort is an important issue in electrical machines. Generally, there are two main techniques to reduce vibration and noise of electrical machines: active techniques by developing a special control of the motors and passive techniques by modifying the motor design—geometry and materials (Vér and Beranek 2008).

Active control permits achieving a reduction of some current harmonics, whose amplitudes are directly proportional to the displacement amplitudes (Riley *et al.* 1999), but it often requires a complex and expensive control system. Passive techniques need no-current control systems and play a key role in improving the acoustical behavior of electrical machines. As for these passive techniques, two strategies are usually followed: the geometric redesign of the machine to change

*Corresponding author, Ph.D., E-mail: 45050524@163.com

its resonance frequencies (Ojeda *et al.* 2009, Lee *et al.* 2009, Bahramgiri *et al.* 2006, Kuo *et al.* 2003) or the use of materials with some particular damping characteristics. These materials have viscoelastic mechanical properties that are a function of the frequency, and often are multi-layer acoustic structure which composed of perforated plates, airspaces and porous materials. However, the acoustic absorption of these multi-layer acoustic structures is mainly dependent on their fabrication.

A new method—biomimetic method has developed to compensate some defect in industry. Biology has perfected its designs and formed many fruitful abilities through evolution of billions of years. Efficient and reliable technologies and achievements can be developed by adopting the features of natural creations (Xue *et al.* 2007, Han *et al.* 2012, Ren *et al.* 2001, Guo *et al.* 2011, Feng *et al.* 2005). It is suggested that the owl has developed its strategy of a silent predator based on various characteristics of its body surface (Graham 1934, Kroeger *et al.* 1972, Lilley 1998, 2004). At present, in the field of bionics, investigations on the noise reduction characteristics of owl body surface are mainly focused on its morphological features. Sun *et al.* (2008), Liu *et al.* (2004) and Wang *et al.* (2014) considered that the skin and feather of owl chest and abdominal may also play an important role on its silent flight. It was concluded that the noise suppression of the owl chest and abdominal was due to the synergy effect of material, skin structure and feather shape etc., and further named as biological coupling. Inspired by this fact, a bionic coupling multi-layer structure is established in this article according to the bionic analogy principle.

Modal approaches are widely used in automotive industry for analyzing the frequency response of large vibro-acoustic models. Generally, these models involve a body-in-white structure which represented by undamped invacuo modes, coupled to an acoustic cavity and covered by a set of trim components. The efficiency of the modal approach relies on a modal extraction for which efficient eigenvalue solvers are available as well as the fact that the problem in modal coordinates is of reduced size. The handling of trimmed configurations in the same modal context is however more problematic for the following reasons: (1) The elimination or the over-simplification of the trim components is not appropriate; (2) Significant stiffness and mass variations may be introduced by the trim components; (3) Complex frequency-dependent dissipation mechanisms may occur in the various layers of the trim components (Lielens *et al.* 2008).

Due to the involved model size and large number of degrees of freedom of such models, an approach in physical coordinates, though theoretically correct, is not possible. Recently, an updated modal approach has been presented for circumventing the above limitations by Coyette *et al.* (2007). This approach mixes in a hybrid procedure the modal approach for both the structure and the cavity and a physical approach for the trim components. For each trim component, an energetic database is built that describes the component behavior when it is excited by the structural and fluid modes. This database is used to reduce the trim component to updates of the structure and cavity modal parameters so that a solution in modal coordinates can be performed. Various loadcases and trim scenarios are therefore analyzed at a reduced cost. Also random excitations are supported by this method with Van den Nieuwenhof *et al.* (2008). Finally, additional ingredients such as incompatible mesh handling, parallelization and modal filtering techniques can be integrated in order to enhance the performance and the applicability to industrial problems (d'Udekem *et al.* 2008).

Different from that the incident power is calculated on incident and Rayleigh surfaces, radiated powers are calculated on radiating and coupling surfaces using the total acoustic pressure and velocity field. And the radiated power quantities provided for the infinite and modal basis domains or admittance surfaces can be post-processed in the same way than the squared pressure quantity

(Actran/TRIM2016 Users' guide 2016). (Guilloteau *et al.* 2014) analyzed the relationship with the radius of holes and its acoustic radiated power, and presented detailed numerical calculation and experiments. (Sgard *et al.* 2000 and Bécot and Sgard 2006) studied the sound radiated of porous materials and that backed with an air gap. And to my knowledge, there has not yet people study sound radiation of multilayer structure.

Traffic noise is the vast majority of urban noise, besides the automobile noise as the biggest pollution source, a number of other vehicles, such as funicular, ski cabin, etc. should also be taken seriously. The paper develops an absorption structure through biomimetic method and chooses a ski cabin as carrier, presents the acoustic performance of the multi-layer absorption structure and details the updated modal approach. The updated modal approach implemented in Actran/Trim (Actran/TRIM2016 Users' guide 2016) is applied on a simplified ski cabin model with various trim components pasted. The effect of each trim component on the admittance radiated power and SPL at the skier's ears is investigated. It is also shown how a post-processing of the energetic databases related to each trim component delivers additional information on the specific effect of each trim component.

2. Materials and methods

2.1 Establishment of the bionic model

Sun *et al.* (2008) investigated the acoustic performance of the chest and abdominal skin and feather samples of 3 different birds (long-eared owl, pheasant and pigeon). Some bionic characteristics of long-eared owl are displayed in Fig. 1.

By comparing the absorptions and bionic characteristics of owl, the bionic analogies are characterized as follows: (1) The covering feather is analogous to rigid micro-slit plate; (2) The chest fluff is analogous to uniform fiber absorption material; (3) The dermis layer and subcutaneous cavity are analogous to a sound absorber, which compose of flexible micro-perforated membrane and airspace. Fig. 2 presents the bionic coupling structure (a); and some comparative models (b). where model 1 is composed of a micro-slit plate backed with airspace, model 2 is composed of a micro-slit plate backed with porous material, model 3 is a micro-slit plate and micro-perforated membrane, model 4 is multi-layer structure of micro-slit plate, porous material and airspace and model 5 is a multi-layer structure of micro-slit plate, porous material, micro-perforated membrane and airspace. The first four are contrast models and the fifth is the bionic model.

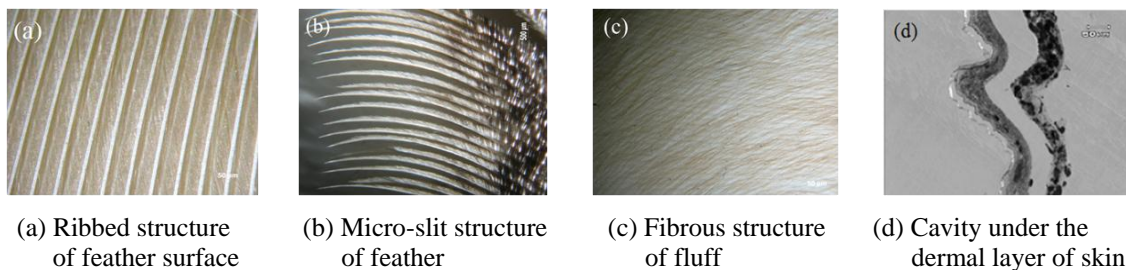


Fig. 1 Some bionic characteristics of long-eared owl (Sun *et al.* 2008)

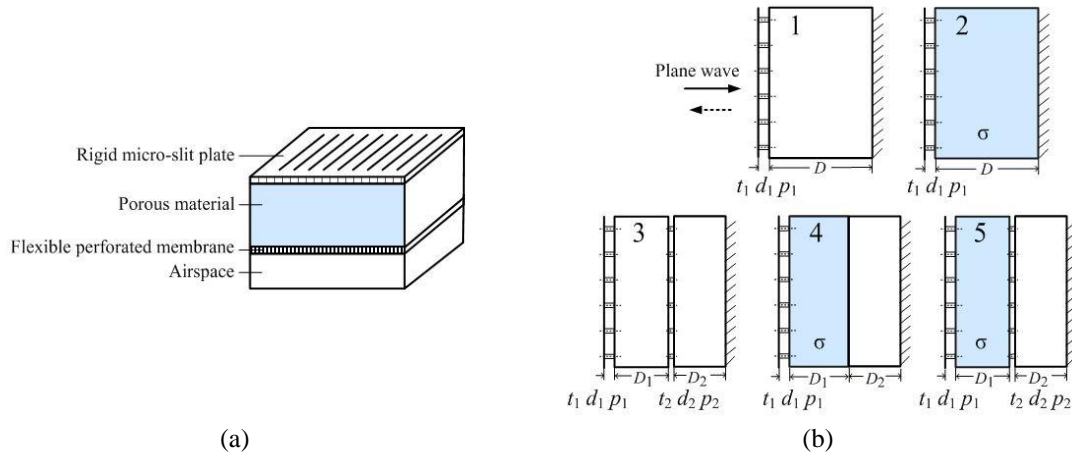


Fig. 2 Bionic absorption structure and comparative models

By comparing the absorptions and bionic characteristics of owl, the bionic analogies are characterized as follows: (1) The covering feather is analogous to rigid micro-slit plate; (2) The chest fluff is analogous to uniform fiber absorption material; (3) The dermis layer and subcutaneous cavity are analogous to a sound absorber, which compose of flexible micro-perforated membrane and airspace. Fig. 2 presents the bionic coupling structure (a); and some comparative models (b). where model 1 is composed of a micro-slit plate backed with airspace, model 2 is composed of a micro-slit plate backed with porous material, model 3 is a micro-slit plate and micro-perforated membrane, model 4 is multi-layer structure of micro-slit plate, porous material and airspace and model 5 is a multi-layer structure of micro-slit plate, porous material, micro-perforated membrane and airspace. The first four are contrast models and the fifth is the bionic model

$$\frac{\partial \rho}{\partial t} + \nabla \cdot (\rho v) = 0 \tag{1}$$

Where ρ is the density of fluid, v is the velocity vector. Euler Equation is

$$\frac{dv}{dt} = -\frac{\nabla p}{\rho} \tag{2}$$

Where p is pressure, d/dt is total derivative operator.

Assuming fluid is irrotational, the velocity vector v is expressed as the gradient of a scalar function ϕ , that is the velocity potential function $v = \nabla \phi$, and substitute it into the Continuity Equation and the Euler Equation, we get

$$\frac{1}{\rho} \frac{\partial \rho}{\partial t} + \frac{\nabla \phi \cdot \nabla \rho}{\rho} + \nabla \phi = 0 \tag{3}$$

$$\frac{\partial (\nabla \phi)}{\partial t} + \frac{\nabla (v^2)}{2} = -\frac{\nabla p}{\rho} \tag{4}$$

Where $v = |v|$. According to the thermodynamic equation and momentum conservation equations, the equation that velocity potential should satisfy can be induced as

$$\nabla \phi - \frac{\nabla p}{\rho} \frac{1}{a^2} \left[\frac{\partial^2 \phi}{\partial t^2} + \frac{\partial}{\partial t} (\nabla \phi \cdot \nabla \phi) + \frac{1}{2} \nabla \phi \cdot (\nabla \phi \cdot \nabla \phi) \right] = 0 \quad (5)$$

Where a represents local sound speed. Acoustic wave propagation theory is applied to the speed and velocity potential, obtaining the acoustic wave equation considering the fluid flow

$$\begin{aligned} \nabla \varphi_a = \frac{1}{a_0^2} \left[\frac{\partial^2 \varphi_a}{\partial t^2} + 2v_0 \cdot \left(\frac{\partial \varphi_a}{\partial t} \right) + \frac{1}{2} \nabla \varphi_a \cdot \nabla (v_0^2) + v_0 \cdot \nabla (v_0 \cdot \nabla \varphi_a) \right] + \\ \frac{1}{a_0^2} (\gamma - 1) \left(\frac{\partial \varphi_a}{\partial t} + v_0 \cdot \nabla \varphi_a \right) (\nabla \cdot v_0) = 0 \end{aligned} \quad (6)$$

Where $v_0 = \nabla \phi_0$ is the mean flow velocity. The general wave equation can be obtained by ignoring the fluid velocity

$$\nabla \phi_a = \frac{1}{a_0^2} \frac{\partial^2 \phi_a}{\partial t^2} \quad (7)$$

Where $v_0 = \nabla \phi_0$ is the mean flow velocity. The general wave equation can be obtained by ignoring the fluid velocity

$$\rho_a = -\rho_0 + \left(\frac{a_0^2}{K_\gamma} \right)^{\frac{1}{\gamma-1}} \left[1 - \frac{\gamma-1}{a_0^2} \left(\frac{\partial \phi_a}{\partial t} + v_0 \cdot \nabla \phi_a \right) \right]^{\frac{1}{\gamma-1}} \quad (8)$$

Sound pressure can be obtained through Taylor series expansion

$$P_a(x,t) = -\rho \frac{d\phi_a(x,t)}{dt} = -\rho [i\omega \tilde{\phi}_a(x) + v_0(x) \cdot \nabla \tilde{\phi}_a(x)] e^{i\omega t} \quad (9)$$

Decompose the fluid density and velocity and introduce potential function transformation $\psi = \bar{\rho}_0 \phi_a$, variation formula can be obtained according to the acoustic propagation theoretical derivation

$$\begin{aligned} \forall \delta \phi = - \int_{\Omega} \frac{\rho_0}{\bar{\rho}_0^2} (\nabla \psi \cdot \nabla \delta \psi - \left(\frac{v_0}{a_0} \cdot \nabla \psi \right) \left(\frac{v_0}{a_0} \cdot \nabla \delta \psi \right)) d\Omega - i\omega \int_{\Omega} \frac{\rho_0}{a_0^2 \bar{\rho}_0^2} (\delta \psi (v_0 \cdot \nabla \psi) - \\ \psi (v_0 \cdot \nabla \delta \psi)) d\Omega + \omega^2 \int_{\Omega} \frac{\rho_0}{a_0^2 \bar{\rho}_0^2} \psi \delta \psi d\Omega = - \int_{\Gamma} \frac{1}{\bar{\rho}_0^2} \delta \psi (\rho_0 \nabla \psi - \frac{\rho_0}{a_0^2} (i\omega \psi + v_0 \cdot \nabla \psi) v_0) \cdot nd\Gamma \end{aligned} \quad (10)$$

The relationship between admittance, speed and sound pressure of sound absorption boundary is

$$i\omega u_n = A_n P \quad (11)$$

Where A_n is normal admittance, p is represented by b

$$P = \frac{\rho_0}{\bar{\rho}_0} (i\omega\psi + v_0 \cdot \nabla\psi) \quad (12)$$

Variational equation gives the following equations by using Galerkin method

$$(-K - i\omega C + \omega^2 M)\psi = F \quad (13)$$

Where K , C and M are assembled by the cell matrix, F unit is combined by load items, that is $F = \sum_e F^e$.

2.4 Model frequency analysis with FEM

All resonance frequencies and all possible deformations of the structure can be computed with the modal analysis which only depends on the design parameters, the degree-of-freedom constraints, and the material properties. Thus, in this paper, the authors apply this analysis to five different structures for determining the parameter impacts on the global displacement given by each modal contribution.

2.4.1 Calculation principle of model frequency analysis

The equation of the motion for an undamped system, expressed in matrix notation, is written as

$$[M]\{a\} + [K]\{d\} = 0 \quad (14)$$

Where $[M]$ and $[K]$ are the mass matrix and the stiffness matrix of the system, respectively, while vectors $\{a\}$ and $\{d\}$ are the acceleration and the displacement at each node of the mesh, respectively.

For a linear system, free vibrations will be made up of harmonics in the form

$$\{d\} = \{f\}_i \cos \omega_i t \quad (15)$$

Where $\{f\}_i$ is the eigenvector representing the mode shape of the i th natural frequency, $\omega_i t$ is the i th natural circular frequency.

By using Eq. (14), Eq. (15) becomes

$$(-(\omega_i)^2 [M] + [K])\{f\}_i = \{0\} \quad (16)$$

The trivial solution $\{f\}_i = \{0\}$ is not of interest. Eq. (16) is thus solvable if

$$\text{Det}([K] - \omega_i^2 [M]) = 0 \quad (17)$$

The solution of the aforementioned characteristic equation yields to the modal frequencies of the system.

Applying the modal superposition theorem described by Huang (Huang *et al.* 2001), the global displacement of a given point is obtained by summing the displacements caused by each mode. The vibration speed is obtained by deriving this sum with respect to time. Consequently, the total

emitted acoustic power depends on all modal contributions. As shown in Bathe (1996), the displacement vector $\{d\}$ at each point is given by

$$\{d\} = \sum_{i=1}^n \{d_i\} \tag{18}$$

Where n is the number of numerical modes that included in the finite- element model and $\{id_i\}$ denotes the modal contributions given by

$$\{d_i\} = y_i \{f_i\} \tag{19}$$

Where y_i is the modal coordinate.

2.4.2 Computing method with FEM (ACTRAN)

A simplified ski cabin model coupled to an inner cavity with various trim components pasted is implemented in the Actran / Trim software, to analyze the modal response and the SPL near the skier’s ears in the cabin. The specific procedure is as follows: Initially, the acoustic impedance and admittance of the multi-layer absorber and the contrast models are calculated by the above methods. Then, the finite element model containing the cavity and three trim components (a floor carpet and two seats) is established (Fig. 3). The trim components are the models 1 to 5 shown in Fig. 2. Fluid-structure coupling occurs on the whole interface between the structure and the cavity. The acoustic calculations of the models were carried out on an acoustic mesh with approximately 30,000 grid points. The largest element length in the meshes is 80 mm. For linear elements, a rule of thumb is to use 8 linear elements per wavelength to capture the acoustic fluctuation. Thus the maximum frequency is driven by the largest element length and is 531 Hz. Therefore the analysis is performed from 1 Hz up to 500 Hz with a step of 1 Hz. Finally, the finite element model is imported into ACTRAN and the boundary condition and acoustic admittance are set.

In this analysis, ski cabin can be considered as a closed acoustic system (cavity system). It will be assumed rigid at its boundary, only the acoustic part will be modeled. A finite fluid component is defined. They are subjected to various noise sources, mainly due to the cabin structure vibrations. The cavity excitation generated by a part of the ceiling vibration is modeled using a simple acoustic velocity load. The SPL is evaluated with virtual microphones located at the skier's ears. A field point post-processing component is created.

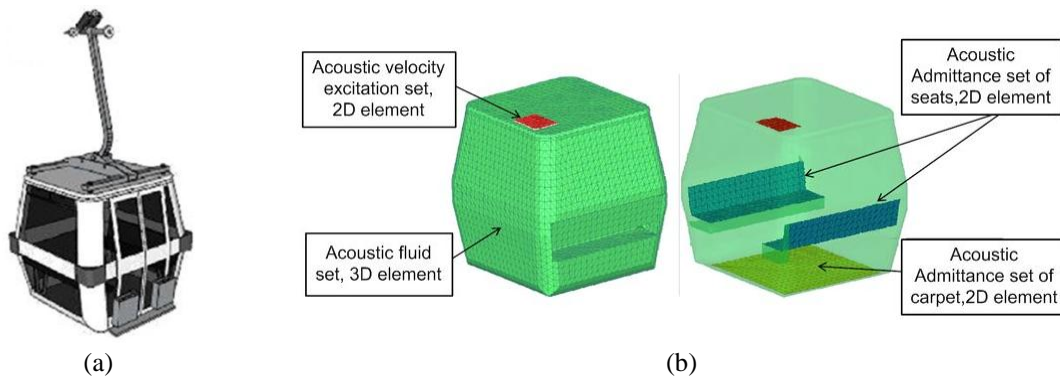


Fig. 3 (a) Ski cabin; and (b) its simplified finite element discrete model

3. Results and discussions

3.1 Modal extraction of a ski cabin cavity

The interior space of the ski cabin is a closed cavity and has modal frequencies and mode shape same with other structural system. The modal of structural system is characterized by a specific distribution of the displacement while acoustic system is based on modal sound pressure distribution. The interior space of the cabin generates acoustic resonance at acoustic mode frequency, which makes the sound pressure magnify. At a certain acoustic modal frequency, sound wave propagates in the cavity of cabin, the reflected wave formed against the boundary superimposed on each other or subtracted, resulting in different sound pressure distribution at different positions, termed for acoustic mode shapes.

When a typical cavity is excited by wallboard, the acoustic resonance will cause annoying low frequency “roaring” noise, and the acoustic modal analysis could provide valuable information for avoiding the acoustic resonant of wallboard and cabin cavity during design phase. The use of three-dimensional model of the cavity sliding cabin can fully reflect its acoustic properties, such as acoustic mode shape for vertical, horizontal, vertical or a combination of different directions.

Therefore, an extraction of the normal modes of the cabin is calculated (Table 1) to characterize the modal behavior of the cabin, and the first twelve modes are shown in Fig. 4. We have to notice that the first eigen value corresponds to the breathing mode of the cavity while others are the mode values.

The conclusion can be drew by comparing each vibration mode that the first order acoustic modal is the longitudinal first-order acoustic modal at 80.1715 Hz. The sound pressures vary longitudinally, and a nodal section appears in transverse section of the longitudinal direction located at the central compartment downwards. The phases on both sides of the nodal section are basically opposite, the sound pressure amplitude gradually increasing and the maximum pressure is situated at the bottom compartment.

The second order acoustic modal is the vertical first-order acoustic modal at 92.7241 Hz. The

Table 1 Acoustic mode results of the cabin

Order	Frequency f /Hz	Modal description
1	8.0171468870220e+01	Longitudinal first order
2	9.2724110728003e+01	Vertical first order
3	9.7565107187724e+01	Transverse first order
4	1.2055639277713e+02	Transverse first order + Longitudinal first order
5	1.2936588839578e+02	Vertical first order + Longitudinal first order
6	1.3538123602370e+02	Vertical first order + Transverse first order
7	1.4820745323870e+02	Longitudinal second order
8	1.6034889563797e+02	Longitudinal first order+ Vertical first order + Transverse first order
9	1.7334016750758e+02	Transverse first order + Longitudinal second order
10	1.7987361121999e+02	Vertical first order + Longitudinal second order
11	1.8485557976039e+02	Vertical second order
12	1.9030839521842e+02	Transverse second order

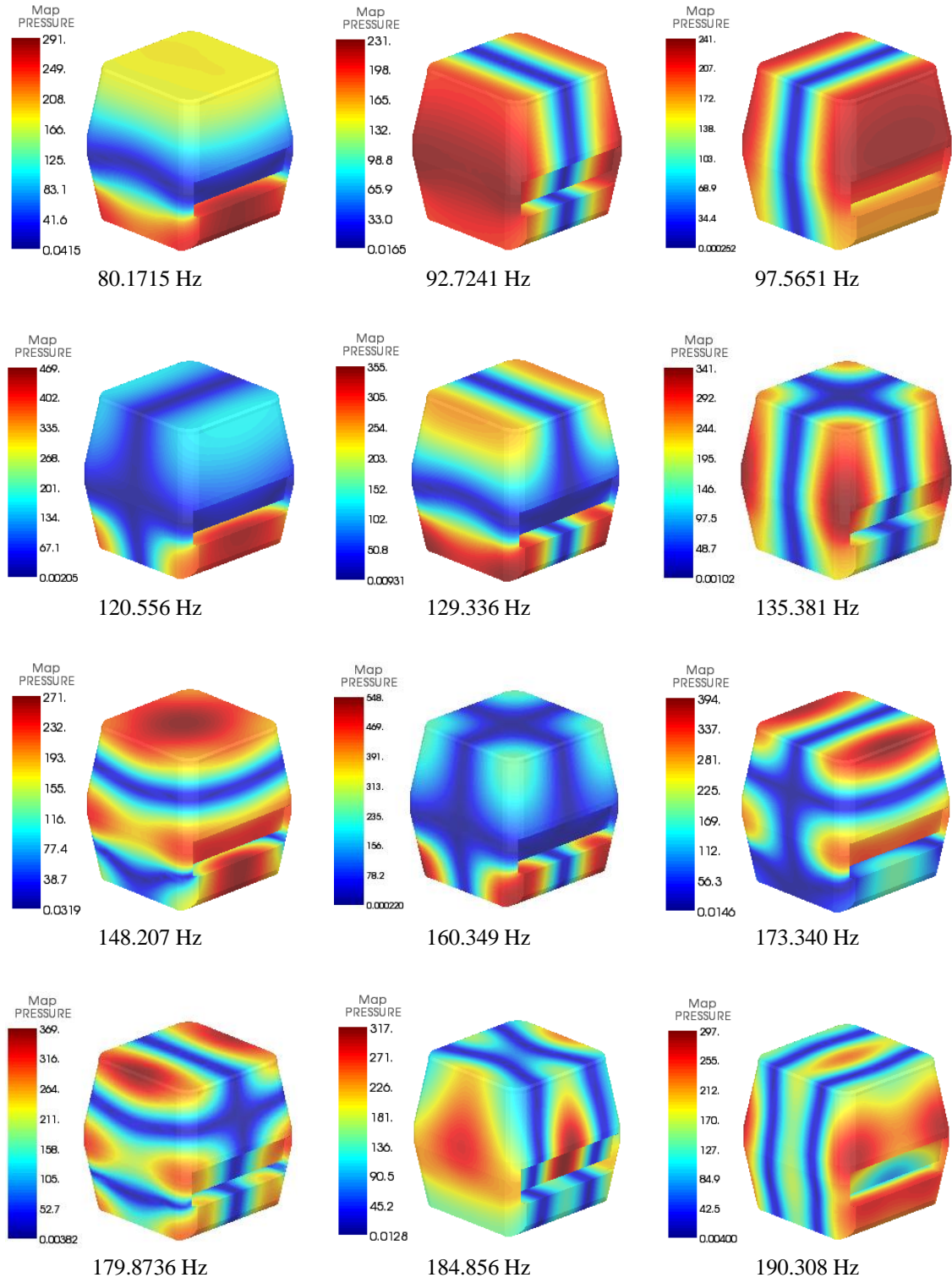


Fig. 4 The first twelve modes of the cabin

sound pressures vary vertically, and a nodal section appears in the longitudinal direction located at the middle section in vertical direction. The phases on both sides of the nodal section are basically opposite, the sound pressure amplitude gradually increasing and the maximum pressure is situated at the middle compartment of side.

The third order acoustic modal is the transverse first-order acoustic modal at 97.5651 Hz. The sound pressures vary transversely, and a nodal section appears in the transverse direction located at the symmetry plane in transverse. The phases on both sides of the nodal section are basically opposite, the sound pressure amplitude gradually increasing and the maximum pressure is situated at the middle seating position.

The fourth order acoustic modal is the superposition of transverse first-order and longitudinal first-order acoustic modals at 97.5651 Hz. The sound pressures vary simultaneously in the longitudinal and lateral directions, and a nodal section appears at the middle section in transverse and longitudinal directions, respectively. The phases on both sides of the transverse nodal section are basically opposite, the sound pressure amplitude gradually increasing and the maximum pressure is situated at the cabin bottom and seats below, totally 2 parts.

The fifth order acoustic modal is the superposition of vertical first-order and longitudinal first-order acoustic modals at 129.336 Hz. The sound pressures vary simultaneously in the longitudinal and vertical directions, and a nodal section appears at the middle section in vertical and longitudinal directions, respectively. The phases on both sides of the vertical nodal section are basically opposite, the sound pressure amplitude gradually increasing and the maximum pressure is situated at the cabin bottom and seats sides, totally 2 parts.

The sixth order acoustic modal is the superposition of vertical first-order and transverse first-order acoustic modals at 135.381 Hz. The sound pressures vary simultaneously in the transverse and vertical directions, and a nodal section appears at the middle section in vertical and transverse directions, respectively. The phases on both sides of the vertical nodal section are basically opposite, the sound pressure amplitude gradually increasing and the maximum pressure is situated at the central location at the junction of cabin sides, totally 4 parts.

The conclusion can be drawn by comparing each vibration mode that the first order acoustic modal is the longitudinal first-order acoustic modal at 80.1715 Hz. The sound pressures vary longitudinally, and a nodal section appears in transverse section of the longitudinal direction located at the central compartment downwards. The phases on both sides of the nodal section are basically opposite, the sound pressure amplitude gradually increasing and the maximum pressure is situated at the bottom compartment.

The second order acoustic modal is the vertical first-order acoustic modal at 92.7241 Hz. The sound pressures vary vertically, and a nodal section appears in the longitudinal direction located at the middle section in vertical direction. The phases on both sides of the nodal section are basically opposite, the sound pressure amplitude gradually increasing and the maximum pressure is situated at the middle compartment of side.

The third order acoustic modal is the transverse first-order acoustic modal at 97.5651 Hz. The sound pressures vary transversely, and a nodal section appears in the transverse direction located at the symmetry plane in transverse. The phases on both sides of the nodal section are basically opposite, the sound pressure amplitude gradually increasing and the maximum pressure is situated at the middle seating position.

The fourth order acoustic modal is the superposition of transverse first-order and longitudinal first-order acoustic modals at 97.5651 Hz. The sound pressures vary simultaneously in the longitudinal and lateral directions, and a nodal section appears at the middle section in transverse

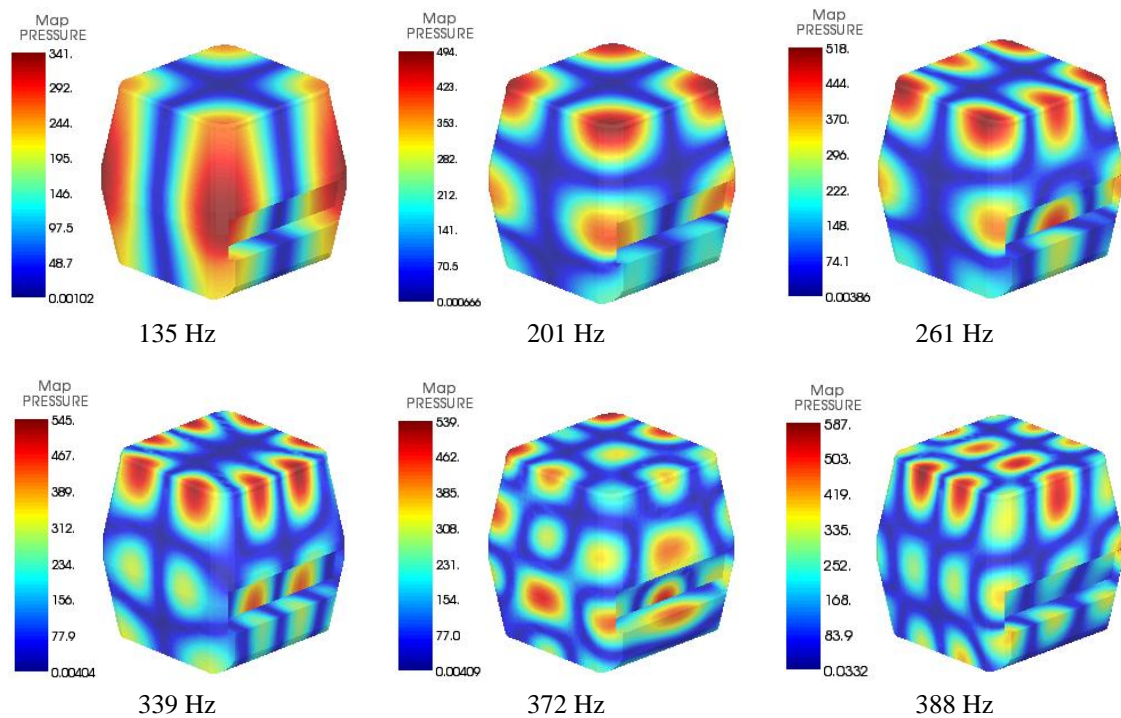


Fig. 5 Modes to be more complex

and longitudinal directions, respectively. The phases on both sides of the transverse nodal section are basically opposite, the sound pressure amplitude gradually increasing and the maximum pressure is situated at the cabin bottom and seats below, totally 2 parts.

The fifth order acoustic modal is the superposition of vertical first-order and longitudinal first-order acoustic modals at 129.336 Hz. The sound pressures vary simultaneously in the longitudinal and vertical directions, and a nodal section appears at the middle section in vertical and longitudinal directions, respectively. The phases on both sides of the vertical nodal section are basically opposite, the sound pressure amplitude gradually increasing and the maximum pressure is situated at the cabin bottom and seats sides, totally 2 parts.

The sixth order acoustic modal is the superposition of vertical first-order and transverse first-order acoustic modals at 135.381 Hz. The sound pressures vary simultaneously in the transverse and vertical directions, and a nodal section appears at the middle section in vertical and transverse directions, respectively. The phases on both sides of the vertical nodal section are basically opposite, the sound pressure amplitude gradually increasing and the maximum pressure is situated at the central location at the junction of cabin sides, totally 4 parts.

3.2 SPL near the skier's ears

The SPL near the skier's ears in the ski cabin within 1-200 Hz is shown in Fig. 6, while the coordinate for the left ear is [3, 0.85, 1.4] and the right ear is [3, 0.65, 1.4]. The obvious resonances can be observed in the SPL results and the first nine peaks SPL that are larger than 140 dB are shown in Fig. 7, which are located at 80 Hz, 93 Hz, 98 Hz, 121 Hz, 130 Hz, 136 Hz, 149

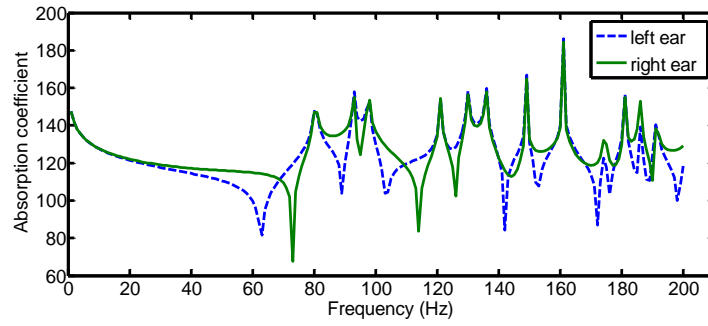


Fig. 6 SPL in dB near the skier's ears in the cabin with no treat

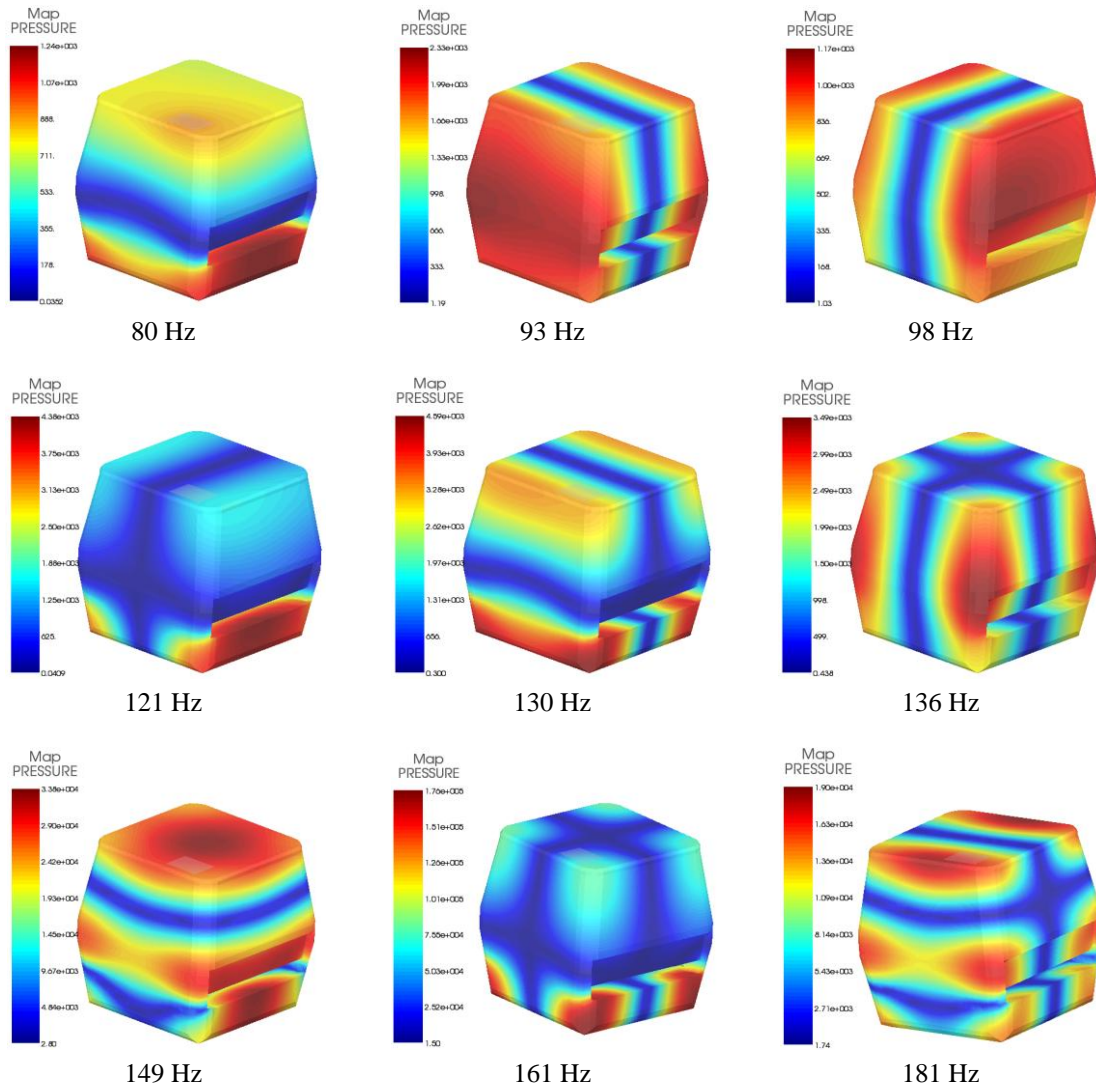


Fig. 7 The first nine peaks SPL that are larger than 140 dB in a cabin

Hz, 161 Hz and 181 Hz. Compared with the modal results in Table 1, all the sound pressure peaks were substantially corresponds to the modal frequencies of the cavity, and also the pressure distribution is similar. Fully showed the importance of modal analysis before the cabin design, we should try to avoid these modal frequencies.

3.3 Sound attenuation in the cabin

The SPL near the skier’s ears is calculated with various models used at both the floor carpet and the seats, and the results are shown in Fig. 8. The results indicated that the SPL near the skier’s ears significantly reduced by adding the five absorption models. In which, model 5 and model 2 expressed the best sound absorption efficiency. The average SPL at point 1 with no treat is 130.5283 dB while that with model 5 is 126.0746 dB and model 2 is 126.0311 dB. In case of point 2, the SPL with no treat is 131.2683 dB while 126.3249 dB and 126.1077 dB for model 5 and model 2, respectively, which means the SPL almost decreased 5 dB.

In order to assess the contribution of each admittance boundary condition, the admittances of carpet and seats are loaded to the ski cabin respectively with model 2 and model 5. The SPL results in a ski cabin with model 5 and model 2 are shown in Figs. 9 and 10, respectively. Depending on the frequency range, the seats and the floor carpet decrease or increase the pressure level in comparison with the untrimmed configuration. The curve related to the configuration in which both trim components are active lies between the curves related to one of the two trim components. As expected, the full admittance configuration is the most efficient to the SPL at the ears of the skier. The carpet contribution seems to be predominant. The spectrum has been shifted

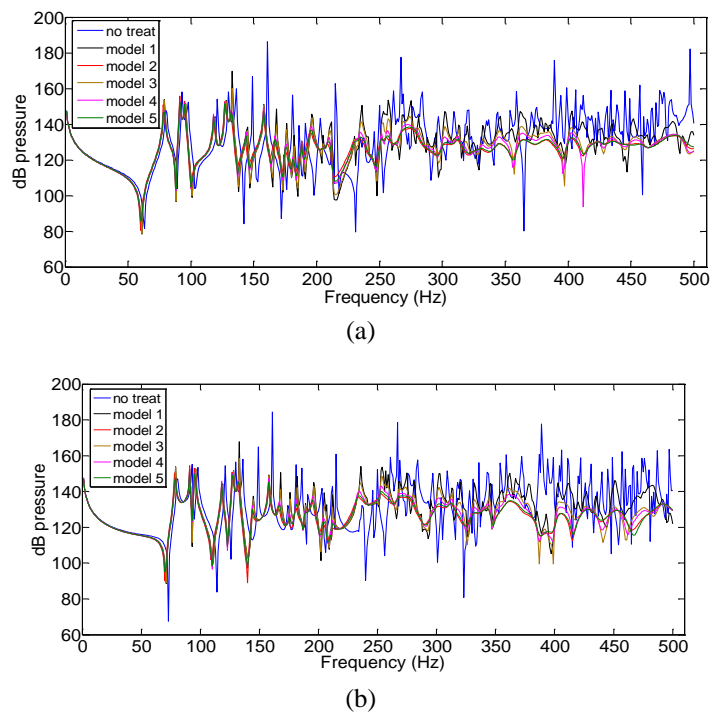
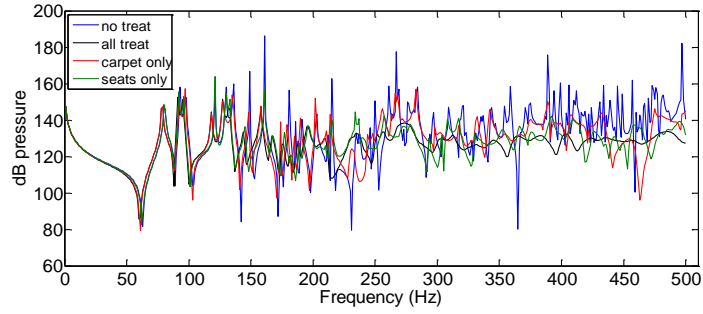
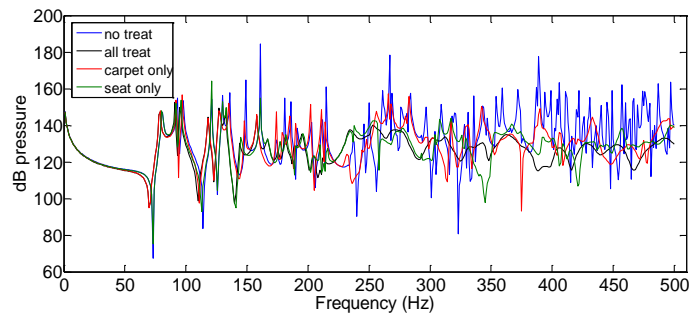


Fig. 8 SPL near the ski’s ears in the cabin with various models

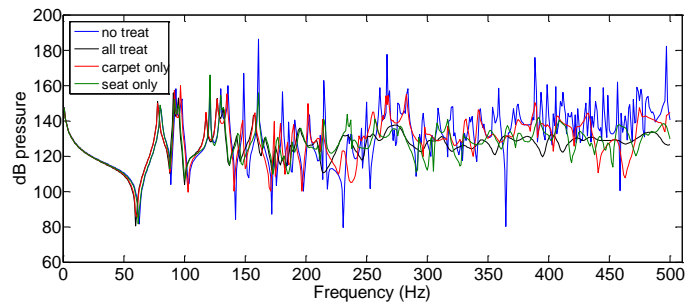


(a)

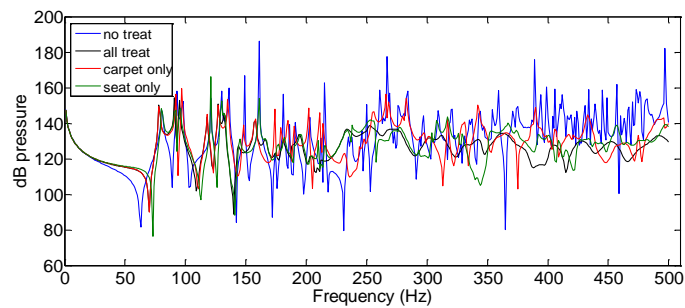


(b)

Fig. 9 SPL near skier's ears in the cabin with model 5



(a)



(b)

Fig. 10 SPL near skier's ears in the cabin with model 2

to the low frequency, which indicates the sound absorption structure increases the system mass. The absorption provided by the absorber is very low in the low frequency range but increases with respect to the frequency.

The admittance radiated power through the free surface with various models is shown in Fig. 11. The admittance radiated power is the sum of the powers dissipated by the power media (various models), such as viscous, thermal, structure and damping, etc. The results revealed that the multi-layer absorption structure do almost not dissipate energy below 50 Hz. The acoustic radiation peaks of five models are almost at the same frequencies. As a whole, model 2 showed the largest admittance radiated power, then model 5 and the lowest for model 1. Compared with the structures of fives models, we can come to the conclusion that maybe the thicker the porous

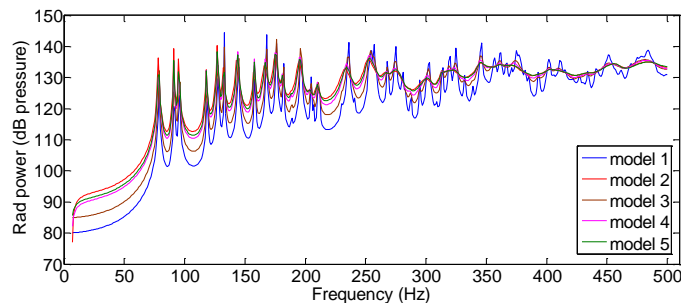
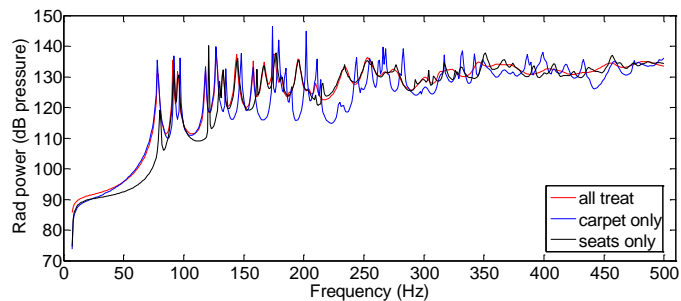
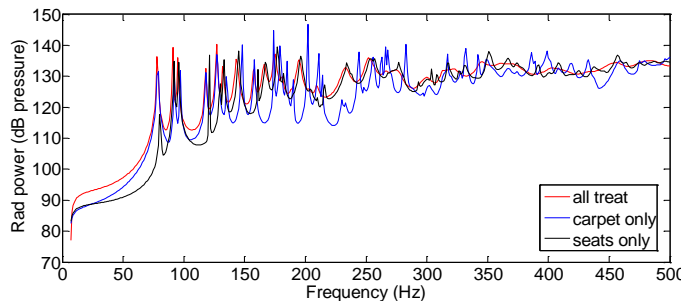


Fig. 11 The admittance radiated power in the cabin with various models



(a)



(b)

Fig. 12 (a) The admittance radiated power in the cabin with model 2; and (b) model 5

material is, the greater the radiation power will be, and the radiant power of the model which contains micro-perforated membrane is larger than model without.

We also present the radiated powers of the ski cabin treated with model 2 and model 5 with all treat, carpet only and seats only in Fig. 12 ((a) is for model 2; (b) is for model 5). The two figures showed the same trends: the ski cabin with all treats presented the largest radiated power, and the carpet treatment is more efficient than the seats treatment. Frequency response highlights same resonance frequencies than the acoustic pressure quantity.

4. Conclusions

In this study, a bionic coupling multi-layer structure is developed based on the biomimetic method. The efficient analysis including modal extraction, sound attenuation and the admittance radiated power in a ski cabin as well as the SPL before and after pasted these models at different components in the cabin are investigated by finite element method (ACTRAN). The acoustic mode and distribution results of the ski cabin showed that it was very important to analyze the modal before the design. We should try to avoid these modal frequencies, so as not to generate low-frequency “roaring” noise and seriously affect comfort for passengers. And the SPL near the ears was significantly reduced after adding sound-absorbing material. Among them, the model 2 and 5 showed the best sound absorption efficiency and SPL almost reduced 5 dB. Moreover, it was most effective for the SPL reduction with full admittance configuration at both the carpet and the seats. The carpet played the dominant contribution. The curve moved to low frequency, which revealed that absorption materials increase the quality of the system. Acoustic absorption provided by the sound absorbing structure in the low frequency was very low, but increased as the frequency increased.

Acknowledgments

All support is greatly acknowledged and appreciated, especially the constructive discussion and criticism from colleagues. Thanks are due to the project of National Natural Science Foundation of China (Grant No. 51505039), and the project of Jilin provincial science and technology department (Grant No. 20150204018GX), and for allowing to undertake the project and the financial support extended.

References

- Actran/TRIM 2016 Users' guide (2016), Free Field Technologies SA, Mont-Saint-Guibert, Belgium.
- Bahramgiri, M., Besmi, M.R., Babaei, M. and Sahebazamani, M. (2006), “A new structure of stator pole to reduce torque ripple and acoustic noise in switched reluctance motor”, *Proceedings of the XVIIth International Conference on Electrical Machines*, Chania, Greece, September.
- Bathe, K.J. (2006), *Finite Element Procedures*, Klaus-Jurgen Bathe.
- Bécot, F.X. and Sgard, F. (2006), “On the use of poroelastic materials for the control of the sound radiated by a cavity backed plate”, *J. Acoust. Soc. Am.*, **120**(4), 2055-2066.
- Coyette, J.P., Lielens, G., Van den Nieuwenhof, B., Bertolini, C., Gaudino, C., Misaji, K. and Ide, F. (2007), “From body in white to trimmed body models in the low frequency range: A new modeling approach (No. 2007-01-2340)”, SAE Technical Paper.

- d'Udekem, D., Acher, F., Khatib-Shahidi, B., Shu, K.T., Rabbani, H. and Liu, W. (2008), "Efficient analysis of a fully-trimmed car body using modal approaches", *INTER-NOISE and NOISE-CON Congress and Conference Proceedings*, Vol. 2008, No. 1, Dearborn, MI, USA, July, pp. 187-195.
- Du, G.H., Zhu, Z.M. and Gong, X.F. (2001), *Acoustic Foundation*, (Second Edition), Nanjing University Press, China.
- Feng, L., Li, S., Li, Y., Li, H., Zhang, L., Zhai, J., Song, Y., Liu, B., Jiang, L. and Zhu, D. (2002), "Super-hydrophobic surfaces: From natural to artificial", *Adv. Mater.*, **14**(24), 1857-1860.
- Graham, R.R. (1934), "The silent flight of owls", *J. Royal Aeronaut. Soc.*, **38**, 837-843.
- Guilloteau, A., Guillemain, P. and Kergomard, J. (2014), "Dependence of the acoustic power produced by a woodwind on the tonehole size", *Proceedings of International Symposium on Musical Acoustics*, Le Mans, France, July, pp. 241-245.
- Guo, Z., Liu, W. and Su, B.L. (2011), "Superhydrophobic surfaces: From natural to biomimetic to functional", *J. Colloid Interf. Sci.*, **353**(2), 335-355.
- Han, Z., Niu, S., Shang, C., Liu, Z. and Ren, L. (2012), "Light trapping structures in wing scales of butterfly *Trogonoptera brookiana*", *Nanoscale*, **4**(9), 2879-2883.
- Huang, S., Aydin, M. and Lipo, T.A. (2001), "Electromagnetic vibration and noise assessment for surface mounted PM machines", *Power Engineering Society Summer Meeting*, Volume 3, Vancouver, BC, Canada, July, pp. 1417-1426.
- Kang, J. and Fuchs, H.V. (1999), "Predicting the absorption of open weave textiles and micro-perforated membranes backed by an air space", *J. Sound Vib.*, **220**(5), 905-920.
- Kroeger, R.A., Grushka, H.D. and Helvey, T.C. (1972), "Low Speed Aero-Dynamics for Ultra-Quiet Flight", Technical Report AFFDL-TR-71-75; Air Force Flight Dynamics Lab, Wright-Patterson Air Force Base, OH, USA.
- Kuo, S.M., Kong, X. and Gan, W.S. (2003), "Applications of adaptive feedback active noise control system", *IEEE T. Contr. Syst. Technol.*, **11**(2), 216-220.
- Lee, F.C. and Chen, W.H. (2001), "Acoustic transmission analysis of multi-layer absorbers", *J. Sound Vib.*, **248**(4), 621-634.
- Lee, S.H., Hong, J.P., Hwang, S.M., Lee, W.T., Lee, J.Y. and Kim, Y.K. (2009), "Optimal design for noise reduction in interior permanent-magnet motor", *IEEE T. Ind. Appl.*, **45**(6), 1954-1960.
- Lielens, G., Van Den Nieuwenhof, B., Acher, F. and Coyette, J.P. (2008), "An energy-based updated modal approach for the efficient analysis of large trimmed models", *J. Acous. Soc. Am.*, **123**(5), 3869.
- Lilley, G.M. (1998), "A study of the silent flight of the owl", *AIAA Paper*, **2340**(1998), 1-6.
- Lilley, G.M. (2004), "A quest for quiet commercial passenger transport aircraft for take-off and landing", *AIAA Paper*, **2922**(10).
- Liu, T.S., Kuykendoll, K., Rhew, R. and Jones, S. (2004), "Avian wings", *AIAA Paper*, p. AIAA-2004-2186.
- Maa, D.Y. (2000), "Theory of microslit absorbers", *Acta Acustica*, **25**(6), 481-485.
- Miki, Y. (1990), "Acoustical properties of porous materials. Modifications of Delany-Bazley models", *J. Acoust. Soc. Japan (E)*, **11**(1), 19-24.
- Ojeda, X., Mininger, X., Ben Ahmed, H., Gabsi, M. and Lécrivain, M. (2009), "Piezoelectric actuator design and placement for switched reluctance motors active damping", *IEEE T. Energy Convers.*, **24**(2), 305-313.
- Ren, L.Q., Tong, J., Li, J.Q. and Chen, B.C. (2001), "SW—Soil and Water: Soil adhesion and biomimetics of soil-engaging components: A review", *J. Agr. Eng. Res.*, **79**(3), 239-263.
- Riley, C.M., Lin, B.K., Habetler, T.G. and Kliman, G.B. (1999), "Stator current harmonics and their causal vibrations: A preliminary investigation of sensorless vibration monitoring applications", *IEEE T. Ind. Appl.*, **35**(1), 94-99.
- Sgard, F.C., Atalla, N. and Nicolas, J. (2000), "A numerical model for the low frequency diffuse field sound transmission loss of double-wall sound barriers with elastic porous linings", *J. Acoust. Soc. Am.*, **108**(6), 2865-2872.
- Sun, S.M., Ren, L.Q. and Xun, C.Y. (2008), "Research on coupling sound absorption property of owl skin and feather", *Noise Vib. Control*, **6**, 119-123. [In Chinese]
- Van den Nieuwenhof, B., Lielens, G. and Coyette, J.P. (2008), "An updated modal approach for dealing

- with vibro-acoustic damped models under random excitation”, *INTER-NOISE and NOISE-CON Congress and Conference Proceedings*, Vol. 2008, No. 1, Dearborn, MI, USA, July, pp. 196-204.
- Ver, I.L. and Beranek, L.L. (2008), *Noise and Vibration Control Engineering, Principles and Applications*, (Second Edition), New York, NY, USA.
- Wang, Y., Zhang, C., Ren, L., Ichchou, M., Galland, M.A. and Bareille, O. (2014), “Sound absorption of a new bionic multi-layer absorber”, *Compos. Struct.*, **108**, 400-408.
- Xue, C., Chen, S., Zhang, W., Zhang, B., Zhang, G. and Qiao, H. (2007), “Design, fabrication, and preliminary characterization of a novel MEMS bionic vector hydrophone”, *Microelectr. J.*, **38**(10), 1021-1026.

CC